Article

Analysis and control of vibrations of a Cartesian cutting machine using an equivalent robotic model

Matteo Bottin [1,*], Giulio Cipriani [1], Domenico Tommasino [1] and Alberto Doria [1]

[1] University of Padova, Department of Industrial Engineering
* Correspondence: matteo.bottin@unipd.it

Received: date; Accepted: date; Published: date

Abstract: The vibrations of a Cartesian cutting machine caused by the pneumatic tool are studied with a sub-system approach. The cutting head is modeled as an equivalent robot arm which is able to mimic the measured resonances, The Cartesian structure is modeled according to the mode superposition approach. The full model is able to predict the variations in the response of the machine to tool excitation that are caused by the motion of the head along the rails of the Cartesian structure. Comparisons with experimental results are made. Finally, the mathematical model is used for assessing the effectiveness of a vibration absorber tuned to main resonance frequency of the cutting head.

Keywords: Vibrations; Cartesian robot; cutting machine

1. Introduction

The Cartesian structure is widely used in robotics and automatic machines. The Cartesian structure offers some advantages, since it is stiffer than a jointed arm structure and kinematically simpler. In many applications, the Cartesian structure can be very large with strokes of many meters. In other applications, the tool mounted on the Cartesian structure may generate large forces or high frequency vibrations that increase noise emission. In these conditions, the analysis and control of vibrations becomes an important issue for a Cartesian machine as well.

In recent years, many studies have focused on the development of control strategies able to achieve in Cartesian robot position control and vibration damping at the same time [1,2]. In particular, in [3] a specific non-linear control was developed to dampen the vibrations of the end-effector caused by the flexibility of the last link and by fast motion in a perpendicular direction. A similar problem was tackled in [2], since each subsystem of a Tripteron robot was modelled as a flexible link driven by a prismatic actuator.

This paper addresses a different problem: the reduction of high frequency vibrations generated by a pneumatic tool mounted on the last link of a Cartesian cutting machine. In this case, the motion caused by the prismatic actuators of the machine does not generate vibrations of the last link, which is rather stiff, but can lead to variations in the response of the structure to high frequency vibrations, since the workspace is rather large and beam flexibility is not negligible.

The paper is organized as follows. In the next section the Cartesian cutting machine is described and the vibration control problem is stated.

In the Section 3 some experimental tests are presented, they were aimed at identifying the vibrational characteristics of the machine and they were carried out with the modal analysis approach [4,5]. The experimental results showed that the motion of the machine can alter the response of the tool to high frequency vibrations, since the stiffness of the rails of the prismatic actuators changes along the workspace.

For this reason, a mathematical model of the machine is developed in the Section 4. The cutting head is modeled adopting a grey-box model identified from experimental tests carried out in a specific location where the rails of the Cartesian structure have the largest bending stiffness. The validity of the model is then extended adding to the grey-box model of the cutting head a dynamic model of the rails.

 doi:10.20944/preprints202107.0072.v1

Section 5 presents the best fitting and validation of the mathematical model. In Section 6 the model is used for analyzing the influence of the modes of vibration of the Cartesian structure on the dynamic response of the cutting head.

In Section 7 the mathematical model is used for assessing the effectiveness of a tuned vibration absorber (TVA) designed to cancel the main resonance of the cutting head. Since the resonance frequency changes in the workspace, a specific tuning taking into account this effect is performed. Finally, conclusions are drawn in Section 8.

2. The Cartesian cutting machine

The machine considered in this work is built to cut sheets of different materials, in particular cloth ones. The machine can be seen in Figure 1.

Figure 1. The machine RAPTOR-HI-2.5 built by Cutting Trading International.

It is constituted of a Cartesian machine that operates over a conveyor belt, supported by four (4) pillars. The sheets are unrolled over the belt and are cut by a cutting head mounted on the sliding rail. This rail is supported at both sides by linear guides. The sliding of the rail and of the cutting head are guaranteed by means of electric motors coupled to elliptical racks and are supported by ball bearing guides. The presence of cables and their support should be taken into account, since they can involve different responses to vibrations on each side of the sliding rail.

The cutting tool is controlled by means of a pneumatic system that, by means of a valve at the input of the tool at high frequency, inflates and deflates air inside a cylinder. This mechanism can guarantee high cutting speed, but at the same time, generates vibrations that may cause annoying noise, especially at high frequencies.

Finally, the machine is modular, so it can be sized to overcome different customer needs.

3. Experimental tests

The dynamic properties of the cutting machine have been identified with the selective modal analysis approach [6], since the machine consists of two well-defined subsystems, shown in Figure 2: the rails of the Cartesian structure and the cutting head.

Preprints (www.preprints.org) | NOT PEER-REVIEWED | Posted: 2 July 2021 doi:10.20944/preprints202107.0072.v1

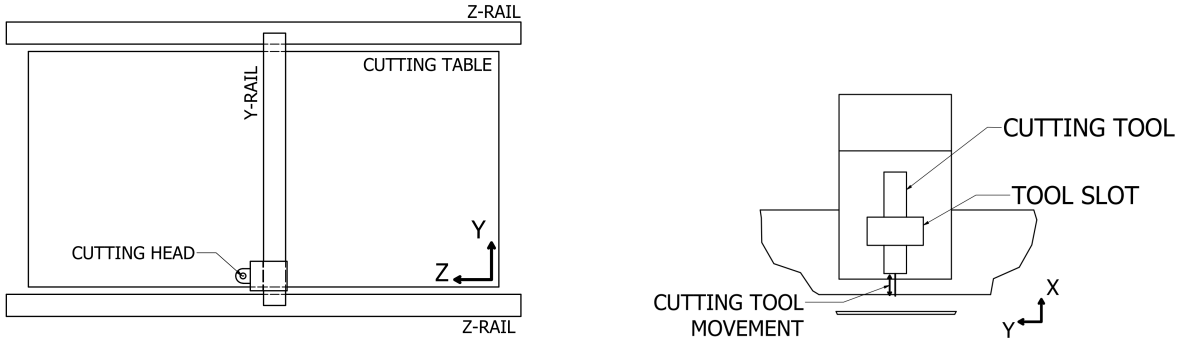

(a) **(b)**

Figure 2. Simplified scheme: a) Cutting machine, b) Cutting head.

This method aims at finding particular configurations of the machine in which only the stiffness properties of a specific subsystem (a joint or a flexible link) are important. In the present case, the Frequency Response Fuctions of the cutting head are measured when the cutting head is located at the border of the workspace and nearly above one of the steel pillars that support the rails. This configuration minimizes the influence of bending deformability of rails.

The tests were carried out using an instrumented hammer for modal testing and a triaxial accelerometer with sensitivities of $0.25\frac{mV}{N}$ and $50\frac{mV}{m/s^2}$ respectively. The measurement points were defined both on the tool and on the rails of the Cartesian machine (Figure 3). This is due to the necessity to assess the influence of the machine characteristics over the vibrations of the tool.

As can be inferred from Figures 4 and 5, the tests for measuring the FRFs on the rails were taken in the worst possible scenario. The one in which the Y-rail and the cutting head are centered on Z-rail and Y-rail, respectively. There are three (3) measurement points on the Z-rail and six (6) on the Y-rail. The Y-rail has more points because it is more flexible and its compliance is directly linked to vibrations of the tool. The red dot in Figures 4 and 5 represents the excitation point that is fixed. Excitation direction is always perpendicular to the rail (X-axis). Measurement direction X is always perpendicular to the rail. The FRFs are calculated averaging the response of three hammer blows.

(a) **(b)**

Figure 3. Experimental setup on the machine. Measurement point: a) on the tool, b) on the rail.

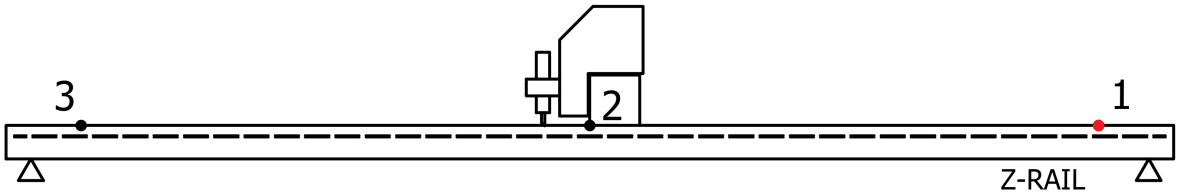

Figure 4. Measurement points on Z-rail, with the red one corresponding to excitation.

Preprints (www.preprints.org) | NOT PEER-REVIEWED | Posted: 2 July 2021 doi:10.20944/preprints202107.0072.v1

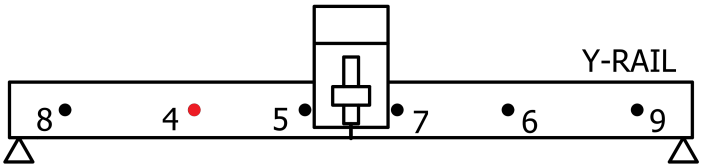

Figure 5. Measurement points on Y-rail, with the red one corresponding to excitation.

In Figures 6a and 6b, the FRFs of Z-rail measured in two different points (1 and 2) are shown. They represent the response of the rail on two points to the excitation in point 1. In both FRFs, the first two peaks occur at about 30 and 50 Hz, respectively, but they are much smaller than the main peak that occurs above 400 Hz.

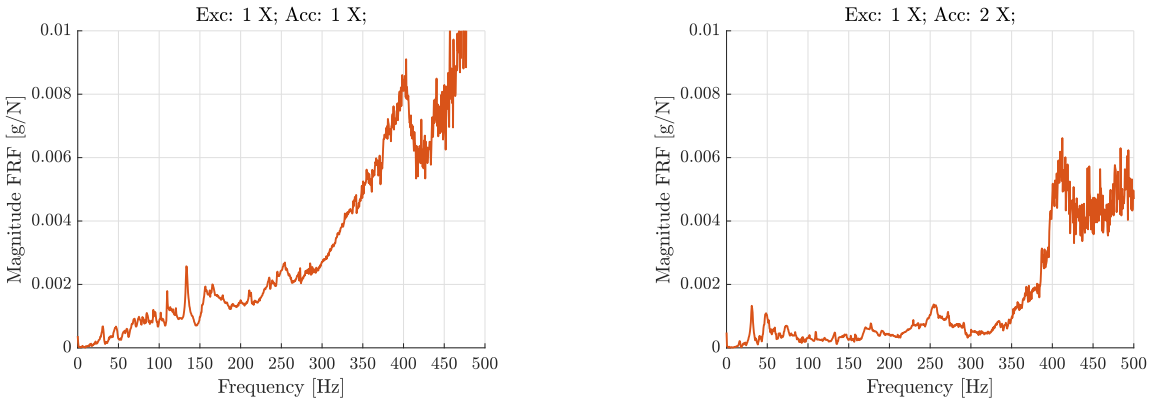

(a) **(b)**

Figure 6. FRFs of Z-rail: a) direct, b) cross at point 2.

Considering Y-rail, Figures 7a and 7b show an high peak at about 23 Hz both in the direct and in the cross FRFs. Moreover, the magnitude is higher than the ones measured on Z-rail. It is important noticing the presence of some peaks around 200 Hz because at this frequency noisy vibrations appear.

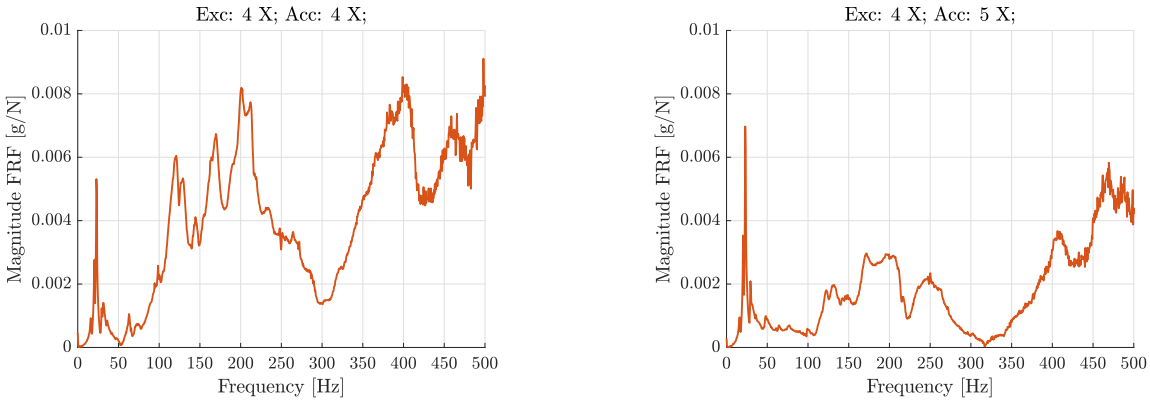

(a) **(b)**

Figure 7. FRFs of Y-rail: a) direct, b) cross at point 5.

In conclusion, it can be stated that Y-rail can have an important influence on the vibrations of the cutting head, whereas the contribution of Z-rail is very weak.

Considering the cutting head, the tests were performed hitting the tool along its vertical (X-axis) and measuring the response vertically (along the accelerometer X-axis) and radially (along the accelerometer Z-axis), following the scheme shown in Figure 8.

Preprints (www.preprints.org) | NOT PEER-REVIEWED | Posted: 2 July 2021 doi:10.20944/preprints202107.0072.v1

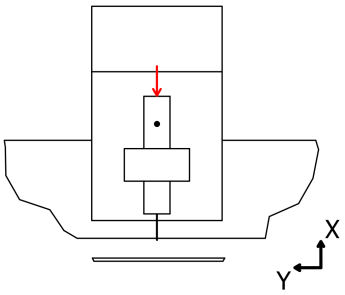

Figure 8. Excitation and measurement point on cutting head.

The cutting head was then moved around the table and different tests were carried out. In Figure 9, the positions of the cutting head are shown (which is displayed in the center-center position). The measured FRFs for some of the points are shown in Figures 10, 11, and 12.

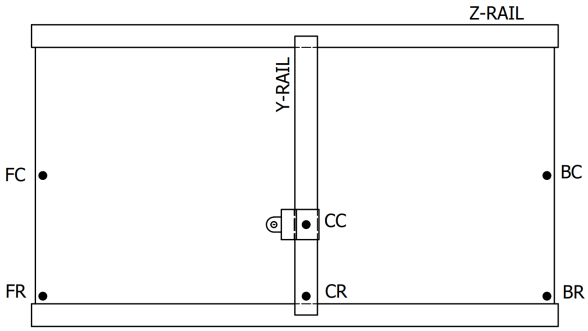

Figure 9. Measure positions for the cutting head, where F = front, C = center, B = back, and R = right.

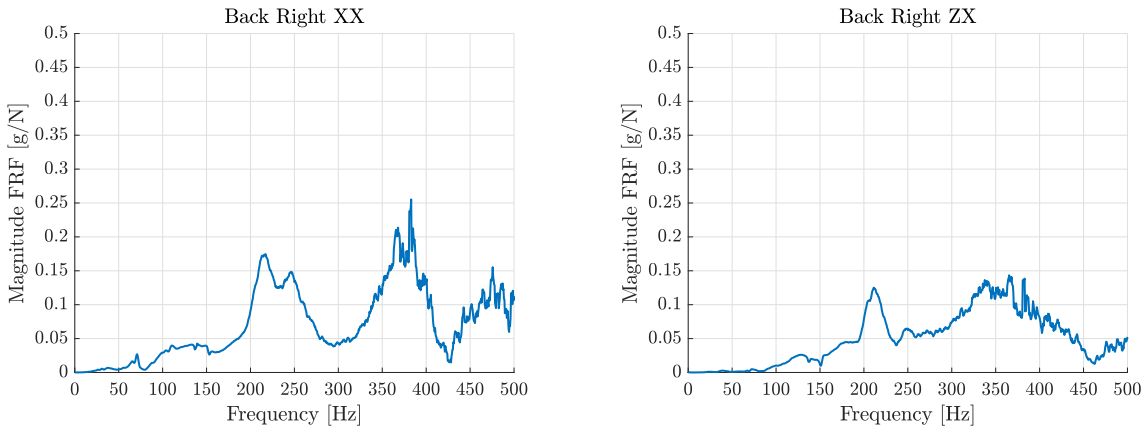

(a) **(b)**

Figure 10. FRFs with the cutting head in the back-right (BR) position.

Direct FRFs show the presence of two close resonance peaks in the range 200-300 Hz; the former with a frequency of 215 Hz, the latter with a frequency of 248 Hz. The relative magnitude of the two peaks depends on the position of the cutting head in the Cartesian workspace. Cross FRFs show a resonance peak at 215 Hz.

4. Mathematical model

The cutting tool moves in the vertical direction (X in Figure 2) and operates at 13000', which corresponds to 217 Hz. Therefore, the features of the measured FRFs about 217 Hz are the most important from the point of view of vibration and noise control.

Preprints (www.preprints.org) | NOT PEER-REVIEWED | Posted: 2 July 2021 doi:10.20944/preprints202107.0072.v1

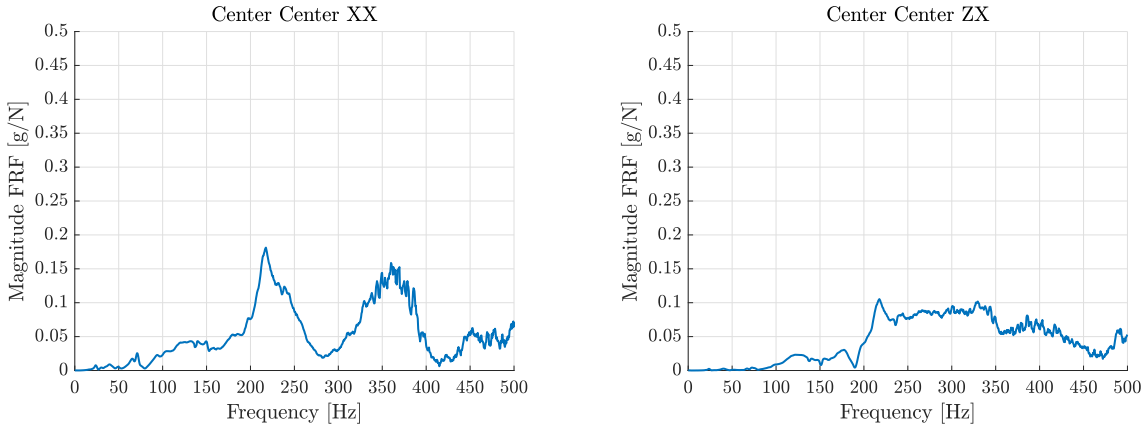

(a) **(b)**

Figure 11. FRFs with the cutting head in the center-center (CC) position.

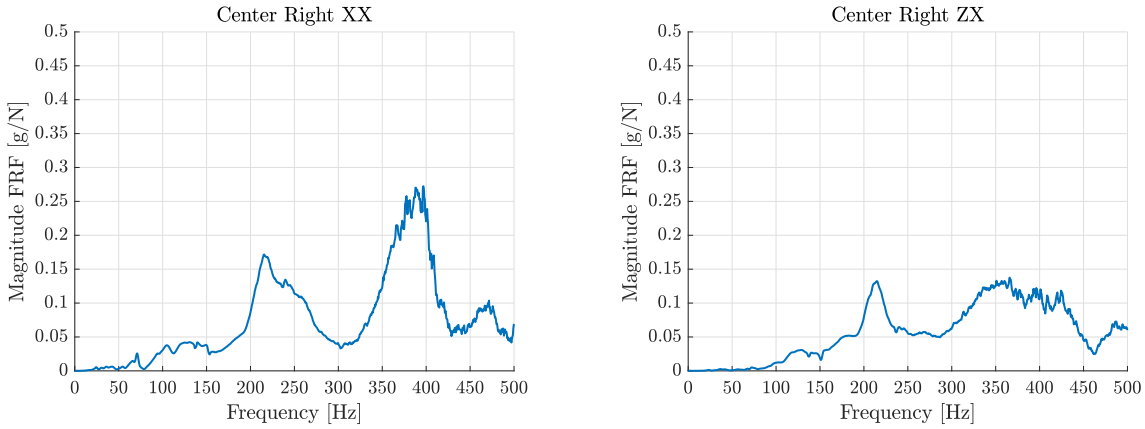

(a) **(b)**

Figure 12. FRFs with the cutting head in the center-right (CR) position.

The mathematical model aims at predicting the response of the cutting machine in the frequency band that includes the maximum excitation for every configuration of the Cartesian robot. The whole cutting machine is divided into two subsystems: the cutting head and the Cartesian robot. A grey-box approach is adopted to model the cutting head. The parameters of this model are not related to the actual geometric and dynamic properties of the cutting head, but are found by means of a best fitting algorithm that minimizes the difference between the measured FRF and the FRF of the equivalent system at a specific location in the workspace.

The stiffness, mass, and damping properties of the Cartesian robot are represented by means of a distributed parameter model developed from the actual drawings of the machine and adopting the mode superposition approach [7]. Actually, the Z-rails are fixed, very bulky and stiff. The modal tests presented in Section 3 showed that they don't have important resonance peaks up to 300 Hz, therefore they can be considered infinitely stiff. Conversely, the Y-rail, which moves at high speed, is lighter and less stiff than the Z-rails. The modal tests presented in Section 3 showed relevant resonance peaks in the range 0-300 Hz that have to be considered in the mathematical model of the cutting machine.

4.1. Cutting head model

Figure 13 shows that the gray-box model of the cutting head is an equivalent jointed-arm robot having 3 Degrees of Freedom.

2 DOFs are associated to rotations θ_1 and θ_2 of the joints with respect to the reference configuration, the third DOF is associated to vertical translation of the robot base x_b, which is due to the compliance

Preprints (www.preprints.org) | NOT PEER-REVIEWED | Posted: 2 July 2021 doi:10.20944/preprints202107.0072.v1

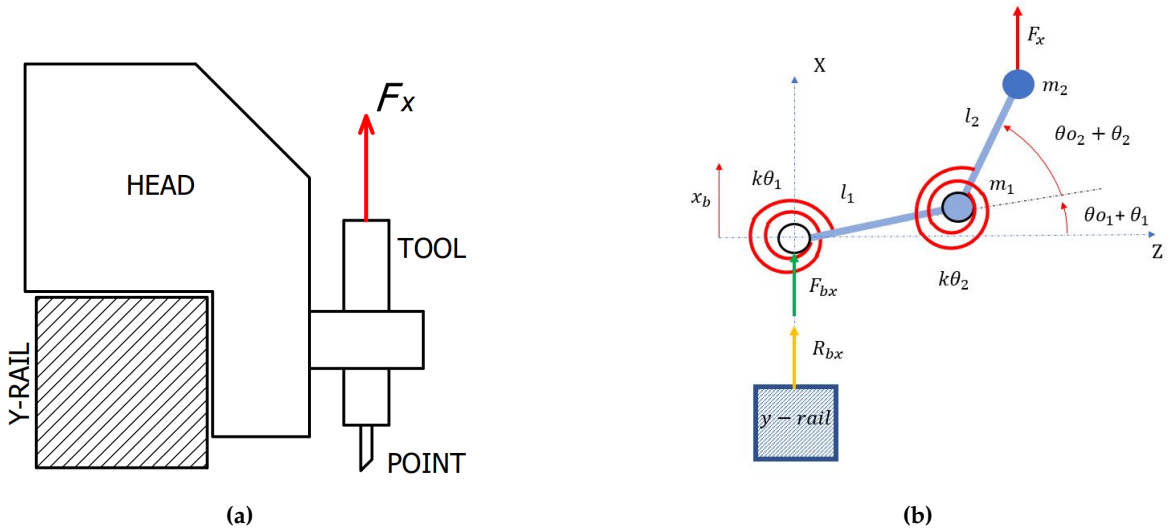

(a) **(b)**

Figure 13. a) physical scheme of the cutting head on the y-rail; b) gray-box model of the cutting machine.

of the rails. The two links having lengths l_1 and l_2 are mass-less and have two tip masses (m_1 and m_2 respectively). Two torsional springs (k_{θ_1} and k_{θ_2}) represent joint compliance. In parallel with the springs there are two rotational dampers (with damping coefficients c_{θ_1} and c_{θ_2}), which represent joint damping, and are not shown in Figure 13. Stiffness k_{θ_1} is related to the stiffness of the cutting head and to the stiffness of the bearing of the prismatic joint between the Y-rail and the cutting head. Mass m_1 is related to the mass of the cutting head. Stiffness k_{θ_2} is chiefly related to the connection between the cutting head and the tool, and mass m_2 is related to the mass of the tool. The joint variables that define the reference configuration of the vibrating robot are important. In particular, joint variable θ_{01} chiefly defines the ratio between vertical (X) and longitudinal (Z) accelerations, whereas joint variable θ_{02}, which is the relative angle between link 2 and link 1 in the reference condition, defines the importance of the inertial cross coupling between the joints [8].

Two external forces act on the equivalent robot. Force F_x is the force in the vertical direction caused by the cutting process, whereas force F_{bx} is the force exerted by the Y-rail on the cutting head.

The equations of motion are derived with the Lagrange method and are expressed in matrix form, gravity forces are neglected:

$$\begin{bmatrix} m_{11} & m_{12} & m_{13} \\ m_{21} & m_{22} & m_{23} \\ m_{31} & m_{32} & m_{33} \end{bmatrix} \begin{Bmatrix} \ddot{\theta}_1 \\ \ddot{\theta}_2 \\ \ddot{x}_b \end{Bmatrix} + \begin{bmatrix} c_{\theta_1} & 0 & 0 \\ 0 & c_{\theta_2} & 0 \\ 0 & 0 & 0 \end{bmatrix} \begin{Bmatrix} \dot{\theta}_1 \\ \dot{\theta}_2 \\ \dot{x}_b \end{Bmatrix} + \begin{bmatrix} k_{\theta_1} & 0 & 0 \\ 0 & k_{\theta_2} & 0 \\ 0 & 0 & 0 \end{bmatrix} \begin{Bmatrix} \theta_1 \\ \theta_2 \\ x_b \end{Bmatrix} = \begin{Bmatrix} Q_1 \\ Q_2 \\ Q_b \end{Bmatrix} \quad (1)$$

Mass matrix is symmetric and includes the inertial cross-coupling terms (the terms outside diagonal):

$$\begin{bmatrix} m_2[l_1^2 + l_2^2 + 2l_1 l_2 cos(\theta_{02})] + m_1 l_1^2 & m_2 l_2[l_2 + l_1 cos(\theta_{02})] & m_2 l_2 cos(\theta_{01} + \theta_{02}) + (m_1 + m_2) l_1 cos(\theta_{01}) \\ m_2 l_2[l_2 + l_1 cos(\theta_{02})] & m_2 l_2^2 & m_2 l_2 cos(\theta_{01} + \theta_{02}) \\ m_2 l_2 cos(\theta_{01} + \theta_{02}) + (m_1 + m_2) l_1 cos(\theta_{01}) & m_2 l_2 cos(\theta_{01} + \theta_{02}) & m_1 + m_2 \end{bmatrix} \quad (2)$$

The damping and stiffness matrices are simple diagonal matrices. The vector at the right hand side includes the effect of the cutting force and of the reaction force that the Y-rail exerts on the cutting head.

Preprints (www.preprints.org) | NOT PEER-REVIEWED | Posted: 2 July 2021 doi:10.20944/preprints202107.0072.v1

$$\begin{Bmatrix} Q_1 \\ Q_2 \\ Q_b \end{Bmatrix} = \begin{Bmatrix} F_x[l_1 cos(\theta_{01}) + l_2 cos(\theta_{01} + \theta_{02})] \\ F_x[l_2 cos(\theta_{01} + \theta_{02})] \\ F_x + F_{bx} \end{Bmatrix} \tag{3}$$

There are four unknowns: $\theta_1(t)$, $\theta_2(t)$, $x_b(t)$ and $F_{bx}(t)$.

4.2. Y-rail model

Figure 14 represents the model of the Y-rail.

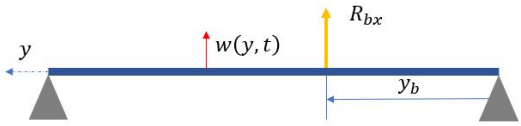

Figure 14. Model of the Y-rail.

The Y-rail, which dominates the vibrational behavior of the Cartesian robot, is modeled as a distributed parameter system by this equation:

$$EI\frac{\partial^4 w(y,t)}{\partial y^4} + c_s I\frac{\partial^5 w(y,t)}{\partial y^4 \partial t} + \mu\frac{\partial^2 w(y,t)}{\partial t^2} = R_{bx}(t)\delta(y - y_b) \tag{4}$$

where $w(y,t)$ is the vertical displacement of any point along the Y-rail, EI is the bending stiffness of the cross-section of the rail, μ is the mass per unit length and c_s is the strain-rate damping coefficient. At the right-hand side there is the forcing term due to the interaction with the cutting head, which is located in position y_b

$$R_{bx}(t) = -F_{bx}(t) \tag{5}$$

and δ is the Dirac delta function.

It is worth noticing that the displacement of the robot base is:

$$x_b(t) = w(y_b, t) \tag{6}$$

Displacement $w(y,t)$ can be expressed according to the mode superposition approach as:

$$w(y,t) = \sum_{r=1}^{\infty} \phi_r(y)\eta_r(t) \tag{7}$$

where $\eta_r(t)$ is the r-th modal coordinate and $\phi_r(y)$ is the r-th mass-normalized mode of vibration. The modes of vibration can be obtained solving the free vibration problem with proper boundary conditions, which are pinned ends in the present case. These modes of vibration hold true even if the beam is proportionally damped. The modes of vibration are associated with the natural frequencies:

$$\omega_r = \left(\frac{r\pi}{L}\right)^2 \sqrt{\frac{EI}{\mu}} \tag{8}$$

where L is rail length.

If 7 is inserted into 4, the equation of forced vibrations is transformed into a set of second order ordinary differential equations:

$$\frac{d^2\eta_r(t)}{dt^2} + 2\zeta_r\omega_r\frac{d\eta_r(t)}{dt} + \omega_r^2\eta_r(t) = R_{bx}\phi_r(y_b) \qquad r = 1, ..., \infty \tag{9}$$

Preprints (www.preprints.org) | NOT PEER-REVIEWED | Posted: 2 July 2021 doi:10.20944/preprints202107.0072.v1

In which ζ_r is modal damping ratio. Actually, if only m modes of vibration of the Y-rail belong to the frequency band of interest, the vibration of the Y-rail can be represented by m equation like 9.

4.3. Coupled model

The model of the equivalent robot is coupled with the model of the beam considering that:

$$x_b(t) = \sum_{r=1}^{m} \phi_r(y_b)\eta_r(t) \tag{10}$$

A system of $3+m$ linear differential equations in $3+m$ unknowns is obtained, the unknowns being $\theta_1(t)$, $\theta_2(t)$, $F_{bx}(t)$, $\eta_1(t)$, ..., $\eta_m(t)$.

Since the third equation of the equivalent robot makes it possible to express $F_{bx}(t)$ as a function of the other variables, a final system of $2+m$ linear differential equations in $2+m$ unknowns is obtained. The system is recast in matrix form and implemented in MATLAB, assuming a harmonic forcing function:

$$F_x(t) = F_{0x}e^{i\omega t} \tag{11}$$

where F_{0x} and ω are the amplitude and frequency of the cutting force.

The frequency response functions between the coordinates (physical and modal) and the cutting force are calculated solving the linear system with ω in the range $0-1884\frac{rad}{s}$. The FRFs between X and Z displacements of the tool are calculated according to the following equations:

$$\alpha_{XX}(\omega) = \alpha_{\theta_1 X} \cdot l_1 \; cos(\theta_{01}) + (\alpha_{\theta_1 X} + \alpha_{\theta_2 X}) \cdot l_2 \; cos(\theta_{01} + \theta_{02}) + \alpha_{x_b X} \tag{12}$$

$$\alpha_{ZX}(\omega) = -\alpha_{\theta_1 X} \cdot l_1 \; sin(\theta_{01}) - (\alpha_{\theta_1 X} + \alpha_{\theta_2 X}) \cdot l_2 \; sin(\theta_{01} + \theta_{02}) \tag{13}$$

where $\alpha_{\theta_1 X}$ and $\alpha_{\theta_1 X}$ are the FRFs between the rotations θ_1, θ_2 and the cutting force in the X-direction, whereas $\alpha_{x_b X}$ is the FRF between the displacement x_b and the cutting force.

4.4. First guess values of the cutting head model

A best fitting process requires a first guess vector of design variables. The design variables of the equivalent robot model of Figure 13 are: l_1, l_2, m_1, m_2, k_{θ_1}, k_{θ_2}, c_{θ_1}, c_{θ_2}, θ_{01} and θ_{02}. First, guess values of these variables are found considering that two close resonance peaks are obtained when a main vibrating system with natural frequency $\Omega = 2\pi f_n$ is coupled with an ancillary oscillator (AO) tuned to the same frequency. Analytical and experimental results show that the original resonance peak at Ω is substituted by two new resonance peaks, the former at lower frequency, the latter at higher frequency [9,10]. The frequency interval between the two peaks depends on the ratio between the masses of the AO and of the main system (mass ratio). Since the masses and the stiffnesses are related through the natural frequency, the mass ratio can be transformed into a stiffness ratio. To obtain the first guess values of the design parameters, some further simplifications are made: $l_1 = l_2 = l$, $\theta_{01} = 0$ and $\theta_{02} = \frac{\pi}{2}$. With the last assumptions, vertical vibrations depend on θ_1, whereas longitudinal vibration depend on $\theta_1 + \theta_2$.

Since the identification is performed when the cutting head is in a corner of the workspace, where the rails reach the maximum stiffness, the motion of the Y-beam is neglected, and the equations of motion of the free undamped vibration of the equivalent robot become:

$$\begin{bmatrix} 2m_2l^2 + m_1l^2 & m_2l^2 \\ m_2l^2 & m_2l^2 \end{bmatrix} \begin{Bmatrix} \ddot{\theta}_1 \\ \ddot{\theta}_2 \end{Bmatrix} + \begin{bmatrix} k_{\theta_1} & 0 \\ 0 & k_{\theta_2} \end{bmatrix} \begin{Bmatrix} \theta_1 \\ \theta_2 \end{Bmatrix} = \begin{Bmatrix} 0 \\ 0 \end{Bmatrix} \tag{14}$$

Preprints (www.preprints.org) | NOT PEER-REVIEWED | Posted: 2 July 2021 doi:10.20944/preprints202107.0072.v1

The terms of the mass matrix can be expressed as functions of the natural frequencies of the main system and of the AO, which are tuned to the same value $\Omega = 2\pi f_n$. The natural frequency of the main system is:

$$\Omega = \sqrt{\frac{k_{\theta_1}}{m_1 l^2}} \tag{15}$$

Hence, $m_1 l^2 = \frac{k_{\theta_1}}{\Omega^2}$.
The natural frequency of the AO is:

$$\Omega = \sqrt{\frac{k_{\theta_2}}{m_2 l^2}} \tag{16}$$

Hence, $m_2 l^2 = \frac{k_{\theta_2}}{\Omega^2}$.
The mass matrix of the coupled system becomes:

$$[M] = \begin{bmatrix} 2\frac{k_{\theta_2}}{\Omega^2} + \frac{k_{\theta_1}}{\Omega^2} & \frac{k_{\theta_2}}{\Omega^2} \\ \frac{k_{\theta_2}}{\Omega^2} & \frac{k_{\theta_2}}{\Omega^2} \end{bmatrix} \tag{17}$$

If stiffness k_{θ_1} is expressed as a function of stiffness k_{θ_2}:

$$k_{\theta_1} = \kappa k_{\theta_2} \tag{18}$$

the natural frequencies of the coupled system depend only on Ω and κ and are given by these simple equations:

$$f_{1,2} = f_n \sqrt{1 \mp \frac{1}{\sqrt{\kappa + 1}}} \tag{19}$$

Therefore, looking at the measured FRF it is possible to find the frequency of the minimum (f_{min}) between the close peaks and the frequency interval between them. The frequency of the minimum (230 Hz in the present case, see Fig 10a) is used to define the tuning frequency $f_n = f_{min}$. Then, from Equation 19 a value of κ giving an interval between the resonance peaks of the system equal to the measured one can be found. The other first guess parameters are found giving meaningful values to lengths and masses. Damping coefficients are calculated according to the following equation:

$$c_i = \zeta_i 2\sqrt{k_{\theta_i} m_i l^2} \qquad i = 1, 2 \tag{20}$$

and assigning both to the main system and to the AO a damping ratio $\zeta_i = 0.1$.

5. Identification and validation of the mathematical model

The optimization algorithm uses the *fmincon* function available in MATLAB. This function finds the scalar or the vector X which minimizes the objective function FUN. In this case, the aim of the optimization is to determine the values of the design variables which minimize the difference between the measured FRFs, the direct FRF $H_{XX}(\omega)$ and the cross one $H_{ZX}(\omega)$, and the corresponding FRFs, $\alpha_{XX}(\omega)$ and $\alpha_{ZX}(\omega)$, calculated by means of the mathematical model. Hence, the function FUN to be minimized is:

$$FUN = C_X \cdot (k_X^2 \cdot \alpha_{XX}^2(\omega) - H_{XX}^2(\omega)) + C_Z \cdot (k_Z^2 \cdot \alpha_{ZX}^2(\omega) - H_{ZX}^2(\omega)) \tag{21}$$

where C_X and C_Z are two coefficients which adjust the influence of the FRFs, whereas k_X and k_Z are two scale factors. The *fmincon* function starts the research of the optimum values of the parameters

Preprints (www.preprints.org) | NOT PEER-REVIEWED | Posted: 2 July 2021 doi:10.20944/preprints202107.0072.v1

from the first guess values X_0 of the design variables. The solution X of the problem is found within the range defined by the lower (LB) and upper (UB) limit, that is:

$$LB \leq X \leq UB \tag{22}$$

The calculation of the analytical FRFs is based on the 2DOF model of the equivalent robotic system, and this implies that the measured FRFs used for the determination of the parameters of the model must be independent from the stiffness of the rails. Hence, the optimization algorithm is applied to the FRFs measured in the back-right (BR) position of the working table. The first guess values X_0 of the design variables, defined through the approach described in the previous section, are summarized in Table 1.

m_1	m_2	l_1	l_2	θ_{01}	θ_{02}	k_1	k_2	c_1	c_2
$[kg]$	$[kg]$	$[m]$	$[m]$	$[deg]$	$[deg]$	$[Nm^{-1}]$	$[Nm^{-1}]$	$[Nsm^{-1}]$	$[Nsm^{-1}]$
24	0.5	0.1	0.1	0	90	522100	10442	36.84	0.72

Table 1. First guess values of the design variables.

The values of the upper and lower limit of the values of the design variables are summarized in Table 2:

Limit	m_1	m_2	l_1	l_2	θ_{01}	θ_{02}	k_1	k_2	c_1	c_2
	$[kg]$	$[kg]$	$[m]$	$[m]$	$[deg]$	$[deg]$	$[Nm^{-1}]$	$[Nm^{-1}]$	$[Nsm^{-1}]$	$[Nsm^{-1}]$
Lower	23	0.4	0.09	0.09	0	90	469890	9397.8	29.48	0.58
Upper	25	0.6	0.11	0.11	10	110	574310	11486.2	44.21	0.87

Table 2. Lower and upper limit.

The optimized values of the design variables, generated by means the *fmincon* function assuming $C_X = 1$, $C_Z = 0.25$, $k_X = 1$ and $k_Z = 0.1$, are summarized in Table 3.

m_1	m_2	l_1	l_2	θ_{01}	θ_{02}	k_1	k_2	c_1	c_2
$[kg]$	$[kg]$	$[m]$	$[m]$	$[deg]$	$[deg]$	$[Nm^{-1}]$	$[Nm^{-1}]$	$[Nsm^{-1}]$	$[Nsm^{-1}]$
24.88	0.60	0.097	0.096	0.65	110.00	522100	10442	44.20	0.58

Table 3. Optimized values of the design variables.

Figure 15 compares the measured FRFs with numerical the FRFs that are obtained introducing the values of Table 3 in the 2-DOF equivalent robotic model.

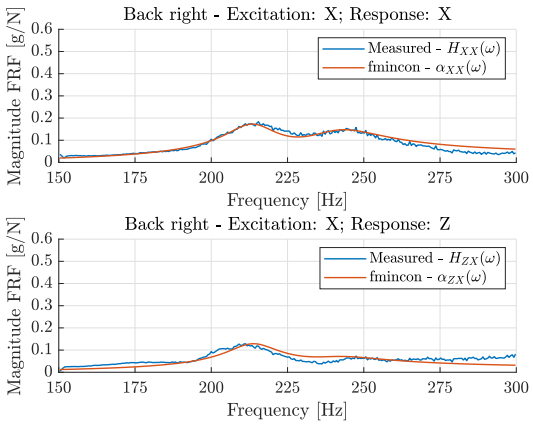

Figure 15. Comparison between the measured FRFs with the FRFs resulting from the optimization algorithm *fmincon*.

Preprints (www.preprints.org) | NOT PEER-REVIEWED | Posted: 2 July 2021 doi:10.20944/preprints202107.0072.v1

Figure 15 shows that the optimization algorithm leads to numerical FRFs which fit very well the measured FRFs. The resonance frequencies are matched and also the trends at the borders of the frequency range are reproduced with high accuracy.

6. Effect of cutting head position

Once defined the parameters of the equivalent robotic model, it is possible to develop the coupled model which accounts for rail dynamics. Figure 16 compares the measured FRFs in different positions of the working table with the FRFs predicted by the coupled model.

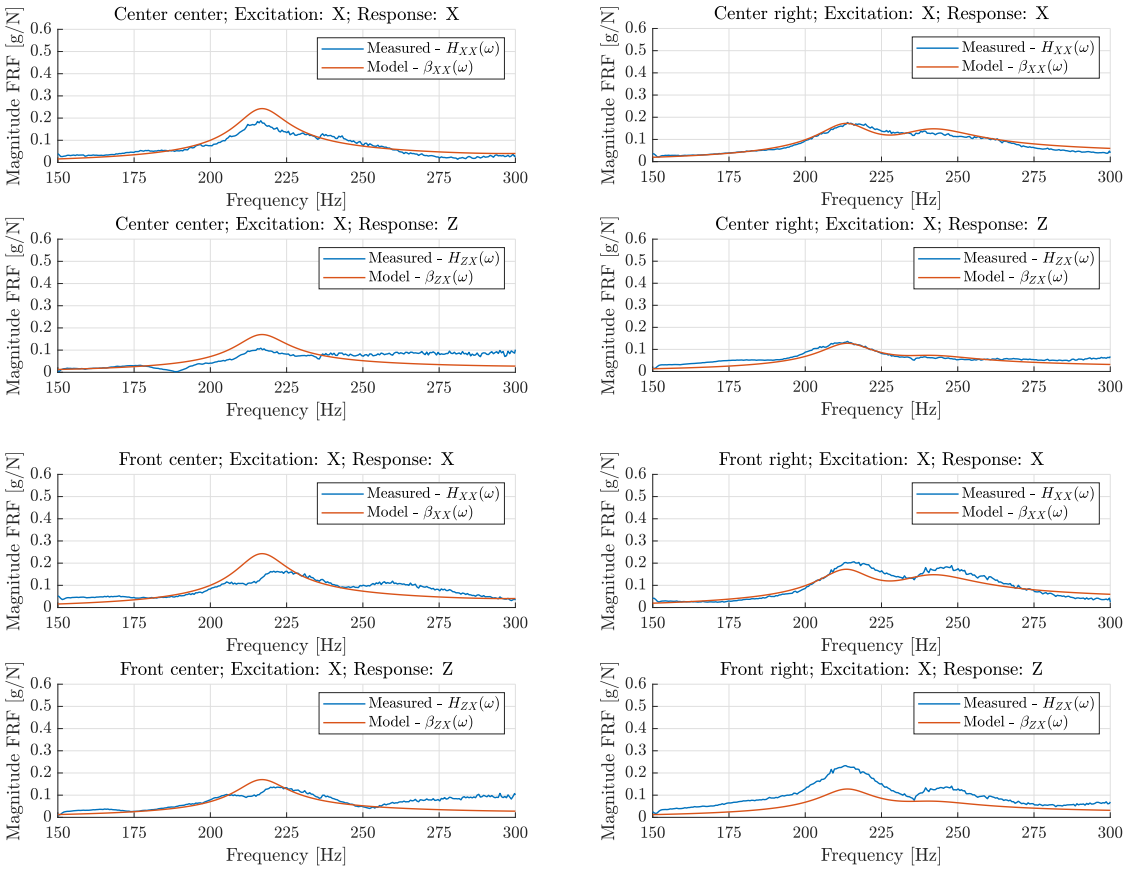

Figure 16. Comparison between the measured FRFs and the numerical FRFs in different positions of the working table.

Figure 16 shows that the model fits the measured FRFs with good accuracy. Moreover, the FRFs change with the position of the cutting head, which means that the dynamics of the rail has an important effect on the whole behavior of the system. The cutting head excites different modes of the Y-rail and the excited modes depend on the position of the head. Figure 17 represents the first four vibration modes of the rail.

A mode of the rail is excited only if the cutting head is not positioned in a node of the mode. This means that the cutting head in the front-centre (FC) or back-centre (BC) position (see Figure 9) will excite only the odds modes of the rail (1^{st} and 3^{rd}), since the cutting head is in the nodes of the even modes (2^{nd} and 4^{th}). Figure 18a shows the FRFs between the r^{th} modal coordinate and the excitation force, when the cutting head is in the front-center (FC) position (or likewise in the back-centre (BR) position), whereas Figure 18b refers to the cutting head in the centre-centre (CC) position, which is approximately at $x_b = L/3$.

Preprints (www.preprints.org) | NOT PEER-REVIEWED | Posted: 2 July 2021 doi:10.20944/preprints202107.0072.v1

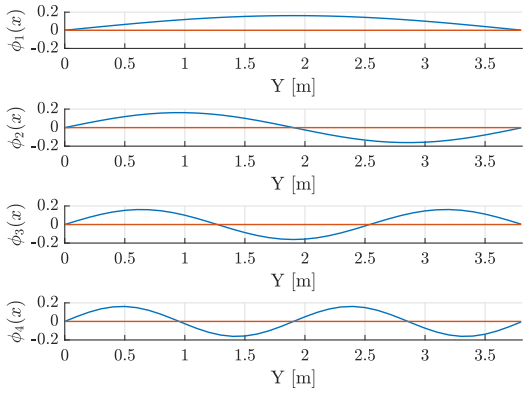

Figure 17. Vibration modes of the y-rail.

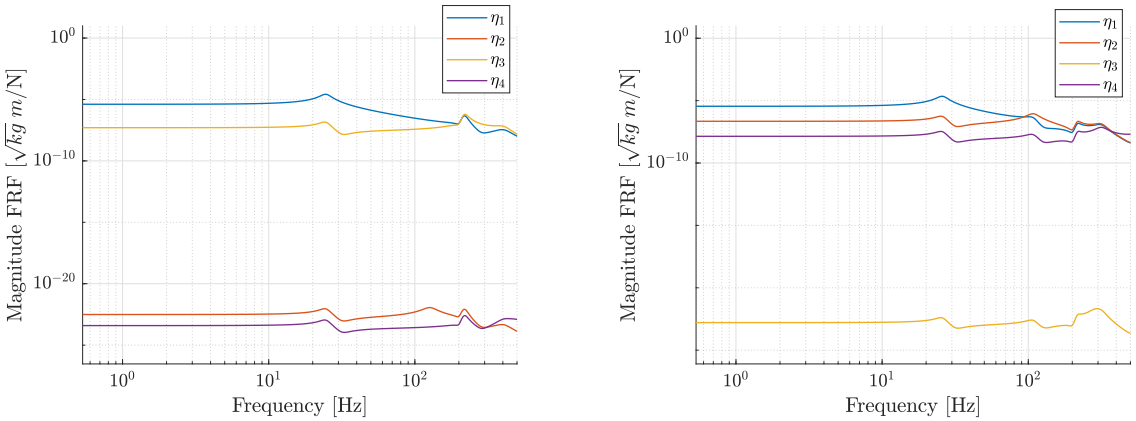

(a) Cutting head in the front-centre (FC) position ($x_b = L/2$).

(b) Cutting head in the centre-centre (CC) position ($x_b = L/3$).

Figure 18. FRFs of the modal coordinate η_r.

In Figure 18a the FRFs relative to the even modes are negligible, since these modes are not excited by the cutting head in the node of the mode. For the same reason, in Figure 18b the third mode is not excited and the corresponding FRF is negligible. This behavior can be seen also in the natural frequencies of the system. Table 4 represents the natural frequencies of the Y-rail without the cutting head, whereas Table 5 represents the natural frequencies of the coupled model, which considers the Y-rail and the cutting head, when the cutting head is in the front-centre (FC) or back-centre (BC) position and when it is in the centre-centre (CC) position.

Mode	Natural frequency [Hz]
1	31.7
2	126.8
3	285.3
4	507.1

Table 4. Natural frequencies of the y-rail without the cutting head.

Table 5 highlights that when the vibration mode of the Y-rail is not excited, the natural frequency of that mode keeps unchanged. Indeed, when the cutting head is in the centre-centre (CC) position, only the natural frequency of the third mode keeps unchanged.

Figure 19 shows the FRF between the acceleration $\ddot{x}_b$ and the cutting force in the X-direction, assuming the cutting head in centre-centre (CC) position.

Preprints (www.preprints.org) | NOT PEER-REVIEWED | Posted: 2 July 2021 doi:10.20944/preprints202107.0072.v1

Mode	Natural frequency in FC or BC [Hz]	Natural frequency in CC [Hz]
1	24.5	25.7
2	126.8	107.9
3	210.6	216.7
4	220.8	285.3
5	409.1	317.2
6	507.1	549.9

Table 5. Natural frequencies of the y-rail with the cutting head in different positions.

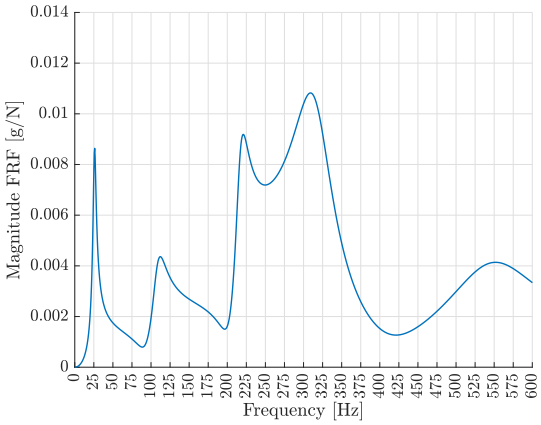

Figure 19. FRF between the acceleration $\ddot{x}_b$ and the cutting force in the X-direction, assuming the cutting head in centre-centre (CC) position.

The Figure corroborates the previous results, since the first two peaks in the FRF are correlated with the first and second vibration mode of the Y-rail with the cutting head in CC position. The vibration mode relative to the thrid mode is not excited, hence it does not appear in the FRF. The thrid and fourth peaks in the FRF are related to the coupled dynamics between the Y-rail and the equivalent robotic arm, whereas the last peak is due to the fourth vibration mode of the y-rail.

7. Control of machine vibration by means of a dynamic vibration absorber

Once the model has been validated, it is interesting to evaluate the effect of vibration control strategies, e.g., the installation of a Tuned Vibration Absorber (TVA). This analysis can be performed using the Sherman-Morrison method [11,12], already shown in [13,14], which makes it possible the calculation of the FRF of the modified system, starting from few FRFs of the original system and the dynamic stiffness of the lumped element $z_l(\omega)$ (the TVA).

In fact, if the TVA is placed at the r^{th} coordinate, each element $a_{pq}(\omega)$ of the receptance matrix can be modified as follows:

$$a_{pqm}(\omega) = \frac{a_{pq}(\omega) + z_l(\omega)(a_{rr}(\omega)a_{pq}(\omega) - a_{pr}(\omega)a_{rq}(\omega))}{1 + z_l(\omega)a_{rr}(\omega)} \tag{23}$$

where $z_l(\omega)$ can be calculated as:

$$z_l(\omega) = \frac{(-\omega^2 m_a k_a - i\omega^3 m_a c_a)}{(k_a - \omega^2 m_a + i\omega c_a)} \tag{24}$$

If the TVA has is tuned at a specific frequency f_N and mass m_a is as a fraction of the mass of the tool M (usually around $0.05 \div 0.1$ M), the stiffness of the TVA can be calculated from the natural frequency of the TVA:

$$k_a = m_a f_N^2 \tag{25}$$

Preprints (www.preprints.org) | NOT PEER-REVIEWED | Posted: 2 July 2021 doi:10.20944/preprints202107.0072.v1

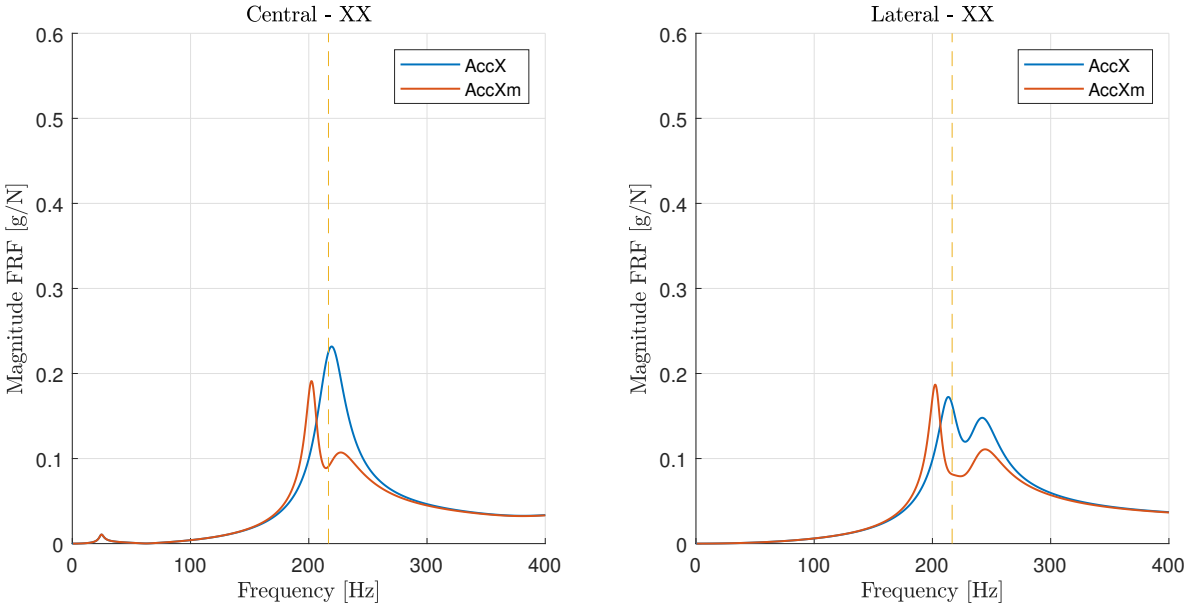

Figure 20. Comparison between the FRF of the model (blue) and the predicted FRF (orange), considering a vibration absorber tuned at $f_N = 212$ Hz, in two different positions of the cutting head. Dashed line shows the working frequency.

Moreover, damping c_a can be calculated according to the damping ratio ζ_a of the material used for the TVA (for a steel beam, $0.01 \div 0.05$):

$$c_a = 2\zeta_a \sqrt{k_a m_a} \tag{26}$$

Let us consider a TVA installed on the tool, designed for controlling vibration in the X direction. Experimental tests and numerical simulations have shown how the FRF slightly changes when the cutting head moves along the rails, however it is not possible to perform structural modifications on-the-fly to account for such FRF changes. Therefore, the TVA has to be appropriately tuned to obtain good results in all the positions of the machine.

Using the FRF predicted by the mathematical model and the Sherman-Morrison method, a parametric analysis was carried out varying the tuning frequency in the range $210 \div 250$ Hz and the damping ratio in the range $0.01 \div 0.05$. The best results were found with the parameters listed in Table 6.

f_N [Hz]	ζ_a	m_a [kg]	c_a [Ns/m]	k_a [N/m]
212	0.04	0.08	8.52	14195

Table 6. Parameters of the TVA.

Figure 20 shows that both in the central position and in the lateral position the TVA is able to minimize the amplitude of the FRF at the forcing frequency of the tool (217 Hz). Unfortunately, the TVA introduces a peak at lower frequencies. This is a well-known behavior of TVAs that is not harmful in this case, since the excitation frequency is rather constant.

The introduction of a peak at lower frequency may be harmful for specific applications, so it is let to the designer to choose whether or not to install the TVA, or rather to change its parameters. In the latter case, it is possible to change the TVA parameters and rapidly simulate a new structural modification by means of the Sherman-Morrison method.

8. Conclusions

A model of the machine is needed to control vibrations and noise in the whole workspace.The experimental test carried out with the modal analysis approach showed that: the fixed rails are very stiff; the moving rail has important resonances in the band of frequency of interest; the the cutting head has two important modes of vibration that can be excited by the pneumatic tool. The mathematical model of the cutting machine is composed of a modal model of the moving rail and of an equivalent robotic model of the cutting head, whose parameters are found by means of a best fitting method that uses only two measured FRFs. This model is able to predict the vibrations of the machine in various locations of the workspace and to assess the usefulness of vibration control strategies, like the installation of a TVA in the tool. The increase in the number of measurement points in the cutting head does not appear very useful, since it could give more information about this vibrating system, but it would require long machine stop times, since many panels and accessories have to be removed to place the accelerometer on the structure of the cutting head. Conversely, the introduction of non-linear elements in the model appears more useful, since the tests showed some asymmetries (e.g., between the left and right side of the machine) that could be modeled only by a non-linear model.

Author Contributions: Conceptualization, G.C. and D.T.; methodology, M.B. and A.D.; software, M.B.; validation, G.C. and D.T.; formal analysis, A.D.; investigation, M.B. and D.T.; data curation, G.C. and D.T.; writing–original draft preparation, M.B. and A.D.; writing–review and editing, M.B., G.C., D.T. and A.D.; visualization, G.C.; supervision, A.D.;

Funding: This research received no external funding.

Acknowledgments: The authors wish to acknowledge the very useful cooperation of Cutting Trading International of Castelfranco Veneto (TV) Italy, that made possible the experimental tests on the machine.

Conflicts of Interest: The authors declare no conflict of interest.

References

1. Boscariol, P.; Zanotto, V. Design of a controller for trajectory tracking for compliant mechanisms with effective vibration suppression. *Robotica* **2012**, *30*, 15–29. doi:10.1017/S0263574711000415.
2. Beiranvand, A.; Kalhor, A.; Tale Masouleh, M. Modeling, identification and minimum length integral sliding mode control of a 3-DOF cartesian parallel robot by considering virtual flexible links. *Mechanism and Machine Theory* **2021**, *157*. doi:10.1016/j.mechmachtheory.2020.104183.
3. Boscariol, P.; Gasparetto, A. Vibration suppression of speed-controlled robots with nonlinear control. *Frontiers of Mechanical Engineering* **2016**, *11*, 204–212. doi:10.1007/s11465-016-0380-3.
4. Doria, A.; Cocuzza, S.; Comand, N.; Bottin, M.; Rossi, A. Analysis of the compliance properties of an industrial robot with the Mozzi axis approach. *Robotics* **2019**, *8*. doi:10.3390/robotics8030080.
5. Ewins, D.J. *Modal testing: theory, practice and application*; John Wiley & Sons, 2009.
6. Bottin, M.; Cocuzza, S.; Comand, N.; Doria, A. Modeling and identification of an industrial robot with a selective modal approach. *Applied Sciences (Switzerland)* **2020**, *10*. doi:10.3390/app10134619.
7. Rao, Singiresu, S. *Mechanical vibrations*; Addison Wesley, 1995.
8. Craig Jr, R.R.; Kurdila, A.J. *Fundamentals of structural dynamics*; John Wiley & Sons, 2006.
9. Doria, A.; Medè, C.; Fanti, G.; Desideri, D.; Maschio, A.; Moro, F. Development of piezoelectric harvesters with integrated trimming devices. *Applied Sciences (Switzerland)* **2018**, *8*. doi:10.3390/app8040557.
10. Liu, H.; Huang, Z.; Xu, T.; Chen, D. Enhancing output power of a piezoelectric cantilever energy harvester using an oscillator. *Smart Materials and Structures* **2012**, *21*. doi:10.1088/0964-1726/21/6/065004.
11. Sanliturk, K. An efficient method for linear and nonlinear structural modifications. Proceedings of ESDA, 2002, Vol. 2002, p. 6th.
12. Çakar, O. Calculation of Receptance of a Structure Modified by Mass and Grounded Spring **2015**.
13. Bottin, M.; Cipriani, G.; Tommasino, D.; Doria, A. Control of the Vibrations of a Cartesian Automatic Machine. *Mechanisms and Machine Science* **2021**, *103*, 236–243. doi:10.1007/978-3-030-75271-2_25.
14. Ozer, M.B.; Royston, T.J. Application of Sherman–Morrison matrix inversion formula to damped vibration absorbers attached to multi-degree of freedom systems. *Journal of sound and vibration* **2005**, *283*, 1235–1249.